Matter

CellPress

Article

Bioinspired Multifunctional Anti-icing Hydrogel

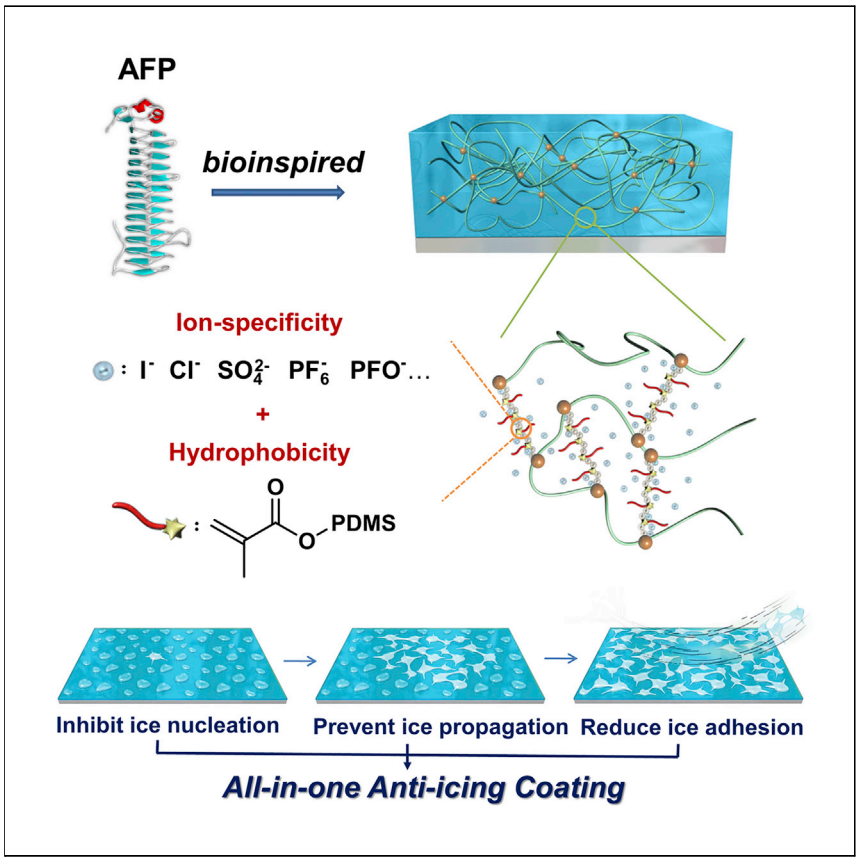

Biological anti-freeze proteins (AFPs) with superior anti-freezing performance offer a great example of perfectly integrating multiple anti-icing functions, by combining hydrogen-bonding and hydrophobic groups to effectively regulate interfacial water. Inspired by AFPs, a multifunctional anti-icing material based on PDMS-grafted polyelectrolyte hydrogel was created.

Zhiyuan He, Chenyang Wu, Mutian Hua, ..., Xinyuan Zhu, Jianjun Wang, Ximin He

xyzhu@sjtu.edu.cn (X.Z.)
wangj220@iccas.ac.cn (J.W.)
ximinhe@ucla.edu (X.H.)

HIGHLIGHTS

Design of the multifunctional anti-icing materials is inspired by anti-freeze proteins

The interfacial water is controlled by tuning the hydrophobicity and ion specificity

Multifunctional anti-icing performance can be achieved with these hydrogels

Improvement
Enhanced performance with innovative design or material control

He et al., Matter 2, 1–12
March 4, 2020
https://doi.org/10.1016/j.matt.2019.12.017

Please cite this article in press as: He et al., Bioinspired Multifunctional Anti-icing Hydrogel, Matter (2019), https://doi.org/10.1016/j.matt.2019.12.017

Matter

CellPress

Article

Bioinspired Multifunctional Anti-icing Hydrogel

Zhiyuan He,[1,2] Chenyang Wu,[2] Mutian Hua,[1] Shuwang Wu,[1,3] Dong Wu,[1] Xinyuan Zhu,[3,*] Jianjun Wang,[2,*] and Ximin He[1,4,*]

SUMMARY

The ice formation processes on solid surfaces are complex and diverse, which makes it a daunting challenge to design an icephobic material that is functional under different icing conditions in a complex varying real-life environment. Here, inspired by anti-freeze proteins, a multifunctional anti-icing platform based on polydimethylsiloxane (PDMS)-grafted polyelectrolyte hydrogel is reported, which can simultaneously inhibit ice nucleation, prevent ice growth, and reduce ice adhesion. The properties of interfacial water can be controlled by tuning the synergy of hydrophobicity and ion specificity, in contrast with the conventional wholly hydrophobic bulk systems (e.g., PDMS). This provides us a promising route to integrate various icephobic advantages into one material. The controllability of interfacial water grants the polyelectrolyte hydrogel coating high performance in inhibiting ice nucleation (ice nucleation temperature lower than −30°C), preventing ice propagation (ice propagation rate lower than 0.002 cm^2/s), and reducing ice adhesion (ice adhesion strength lower than 20 kPa).

INTRODUCTION

Undesired icing/frosting on foreign surfaces causes serious economic, energy, and safety issues and environmental hazards in many areas of society.[1–5] In nature, the complex and diverse ice formation processes, typically from nucleation to subsequent propagation and finally adhesion, always occur over a wide range of temperatures and environmental conditions, resulting in different ice crystals such as glaze, rime, freezing rain, frost, and snow.[6–9] These bring great difficulty to designing icephobic materials facing different icing scenarios in practical applications.[10–12] To solve these problems, great efforts have been made to develop various anti-icing strategies for inhibiting ice nucleation, preventing ice propagation, and reducing ice adhesion.[13–16] Despite the recent rapid development of icephobic materials and methods, each focuses on a single aspect of anti-icing in certain conditions and has obvious limitations for broad practical utility. For example, the superhydrophobic anti-icing surfaces exhibit excellent performance in shedding water, but the disadvantages of durability and humidity tolerance still remain.[17,18] Ion specificity endows polyelectrolyte brushes with unique capabilities of tuning ice nucleation and propagation; however, the poor mechanical robustness limits their application in ice removal.[19,20] Although some hydrated films have ultralow ice adhesion strength due to the aqueous lubricating layer, no excellent anti-icing performance other than reducing ice adhesion has been reported.[21,22] Ideally, an efficient icephobic surface should possess multiple anti-icing features for tackling all the aforementioned obstacles to have true versatility and optimum performance in different possible situations.

Progress and Potential

The recent anti-icing strategies in the state of the art mainly focused on three aspects: inhibiting ice nucleation, preventing ice propagation, and decreasing ice adhesion strength. However, it is has proved difficult to prevent ice nucleation and propagation while decreasing adhesion simultaneously, due to their highly distinct, even contradictory design principles. In nature, anti-freeze proteins (AFPs) offer a prime example of multifunctional integrated anti-icing materials that excel in all three key aspects of the anti-icing process simultaneously by tuning the structures and dynamics of interfacial water. Here, inspired by biological AFPs, we successfully created a multifunctional anti-icing material based on polydimethylsiloxane-grafted polyelectrolyte hydrogel that can tackle all three aspects of the anti-icing process simultaneously. The simplicity, mechanical durability, and versatility of these smooth hydrogel surfaces make it a promising option for a wide range of anti-icing applications.

Creating low-cost, large-scale, high-efficiency, and multifunctional anti-icing material is still a challenge, and few strategies for accomplishing this have been demonstrated.[23–25] However, nature offers many good examples of multifunctional integrated anti-icing control; for example, anti-freeze proteins (AFPs) control ice formation by depressing the freezing temperature, preventing ice growth, and inhibiting ice recrystallization.[2,26] It is reported that all these superior anti-freeze functions are achieved through tuning the structure, mobility, and amount of interfacial water, which respectively regulate the ice nucleation, growth, and adhesion.[27–29] Both hydrogen-bonding and hydrophobic groups contribute greatly to the regulation of interfacial water, thus leading to the AFPs with enhanced anti-freeze activity.[29,30] Recent anti-icing approaches further reinforce the significance of interfacial water in inhibiting ice formation and reducing ice adhesion. For example, Wang et al. revealed that the ions at polyelectrolyte brush interface can effectively control the dynamics of interfacial water and thus determine the ice nucleation and propagation processes.[19,20] Moreover, it was discovered that the ice adhesion strength can be effectively reduced by the aqueous lubricating layer on various hydrated surfaces.[22,31] Ultimately, realizing the regulation of all three aspects of anti-icing with one material simultaneously would require a balance between the optimum structures, mobility, and amount of interfacial water. These properties of interfacial water can be regulated by incorporating and balancing the hydrophilic and hydrophobic components in the materials, as molecular dynamics simulation studies have discovered.[29] Experimentally, tuning one of the above properties has been realized, but it remains a daunting challenge to regulate all three simultaneously, as it requires hydrophilic and hydrophobic synergy at molecular scale within one material. Here, inspired by the strategy of combining hydrogen-bonding and hydrophobic groups in AFPs for the multiple anti-freeze activities, a novel method is proposed to graft hydrophobic polydimethylsiloxane (PDMS) chains onto a hydrophilic polyelectrolyte network containing various counterions, forming a multifunctional hybrid anti-icing hydrogel. By contrast, conventional pure hydrophobic systems without interfacial water present mainly facilitate effectively the ice adhesion but not the nucleation and propagation. Such a unique material design through grafting hydrophobic chains with tunable lengths on hydrophilic charged networks allows for regulation of the properties of interfacial water by tuning the synergy of hydrophobicity and ion specificity, which endows these PDMS-grafted polyelectrolyte hydrogel coatings with high capabilities of tuning the ice nucleation, propagation, and adhesion. The non-structured feature makes these smooth anti-icing surfaces more environmentally tolerant, mechanically robust, and durable.

RESULTS

AFPs have unique capabilities to regulate ice formation process by selectively adsorbing to the ice crystal surface, as shown in Figure 1A. The multiple anti-freezing functions of AFPs are strongly influenced by the interfacial water at the AFP/ice interface, which can be controlled by tuning the arrangement of hydrophobic and charged functional groups.[2,29] Borrowing the concept of AFPs, the rational design of the multifunctional anti-icing hydrogel surface via control of the interfacial water properties is illustrated in Figure 1B. Unlike the existing anti-icing strategies, ours targets an all-around anti-icing material with comprehensive performances in all of these three aspects, i.e., ice nucleation inhibition, ice propagation prevention, and ice adhesion reduction. Hydrogel, which contains different types of interfacial water, provides an ideal platform for tuning interfacial water structure, mobility, and amount, based on chemical modifications. The polymer network of the poly(acrylamide-co-acrylic acid-co-*N*-allylacrylamide) (poly(AAm-co-AAc-co-AAene)) hydrogels offers a scaffold to

[1]Department of Materials Science and Engineering, University of California, Los Angeles, CA 90095, USA

[2]Institute of Chemistry, Chinese Academy of Sciences, Beijing 100190, China

[3]School of Chemistry and Chemical Engineering, State Key Laboratory of Metal Matrix Composites, Shanghai Jiao Tong University, 800 Dongchuan Road, Shanghai 200240, China

[4]Lead Contact

*Correspondence: xyzhu@sjtu.edu.cn (X.Z.), wangj220@iccas.ac.cn (J.W.), ximinhe@ucla.edu (X.H.)

https://doi.org/10.1016/j.matt.2019.12.017

Please cite this article in press as: He et al., Bioinspired Multifunctional Anti-icing Hydrogel, Matter (2019), https://doi.org/10.1016/j.matt.2019.12.017

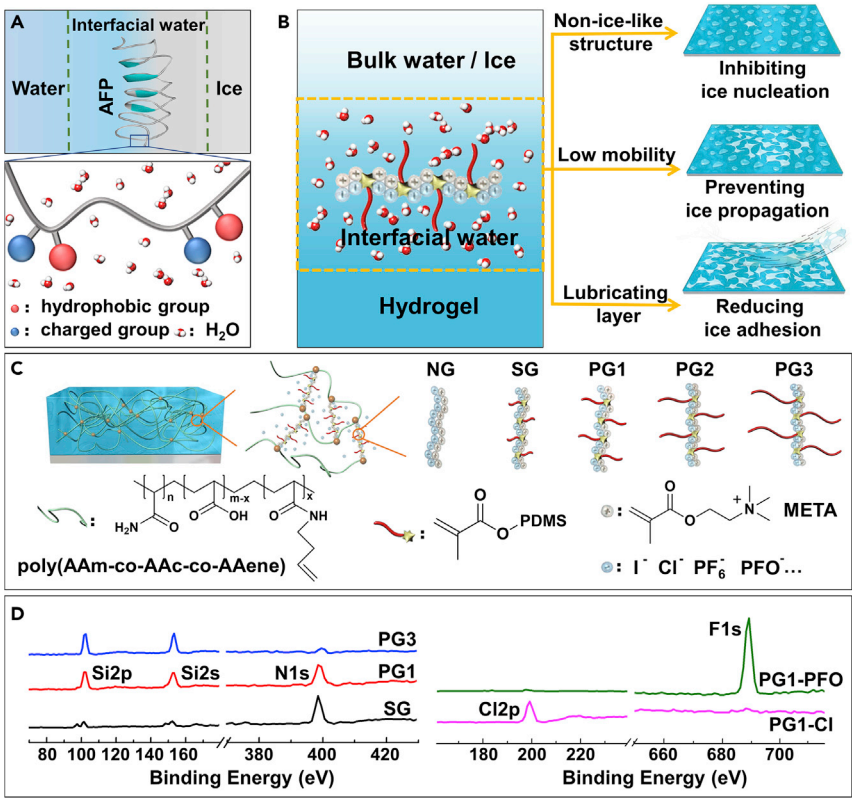

Figure 1. Bioinspired Design of Multifunctional Anti-icing Hydrogel Surfaces

(A) Hydrogen-bonding and hydrophobic groups of AFPs contribute greatly to the regulation of interfacial water.

(B) Inspired by AFPs, a multifunctional anti-icing hydrogel has the capability of controlling ice nucleation, ice propagation, and ice adhesion via tuning structure, mobility, and amount of interfacial water.

(C) The chemical structures of poly(AAm-co-AAc-co-AAene) hydrogels crosslinked by NG (PMETA), SG (PMETA-co-PDMS), PG1 [(PMETA)-g-(PDMS-0.9K)], PG2 [(PMETA)-g-(PDMS-5.7K)], and PG3 [(PMETA)-g-(PDMS-13.2K)], respectively.

(D) XPS spectra of various PDMS-grafted polyelectrolyte hydrogels and the PG1 surface with different counterions.

carry multiple hydrophobic and charged groups (see Figure 1C).[32,33] The copolymerization of cationic [2-(methacryloyloxy)ethyl]trimethylammonium (META) monomer and monomethacrylate-functional PDMS macromonomers of different chain length was carried out using an *in situ* photopolymerization method, forming crosslinks of a series of different graft lengths and compositions (Figures S1 and S2).[34] The poly(AAm-co-AAc-co-AAene) hydrogels were crosslinked by NG (poly[2-(methacryloyloxy)ethyl]trimethylammonium [PMETA]), SG (PMETA-co-PDMS), PG1 ([PMETA]-g-[PDMS-0.9K]), PG2 ([PMETA]-g-[PDMS-5.7K]), and PG3 ([PMETA]-g-[PDMS-13.2K]), respectively. Such a modular design of the polyelectrolyte hydrogel film possesses two unique advantages. The embedded counterions in the hydrogel can be easily exchanged, providing a tunable microenvironment of ion specificity (Figure S3). The other advantage of this film is that the surface hydrophobicity can be readily controlled with the incorporation of various hydrophobic grafted PDMS segments. It is noted that the PDMS-grafted electrolyte hydrogel is fundamentally different from the conventional design: the PDMS chains here are to balance the hydrophilic matrix and thus regulate the interfacial water and also strengthen the intrinsic mechanically weak hydrogel, whereas the conventional PDMS-based

anti-icing materials mainly utilizes its highly hydrophobic nature to repel water. The fine balance of ion specificity and hydrophobicity is pursued here to be able to regulate the interfacial water to an optimum state and leads to the ultimate anti-icing performance improved from the previous pure bulk PDMS and polyelectrolyte surfaces, in terms of freezing temperature, operation window, and condition. The copolymerization and ion exchange were further confirmed by X-ray photoelectron spectroscopy (XPS) as shown in Figure 1D. The thin film of hydrogel is covalently linked to various substrates, with nanometer-scale tunable thickness ranging from ~50 to 1,000 nm (Figures S4 and S5). The film thickness can be recognized easily through the surface color change due to the optical interference effect.[32]

Many scientists have tuned the inhibition of heterogeneous ice nucleation (HIN) before freezing by modifying material surface chemistry and morphology, since HIN is the initial and controlling step of ice formation.[35,36] The delay of HIN provides favorable conditions for the removal of impacting or condensed supercooled water droplets by using different methods.[37,38] Recently, it was found that the efficiency of different ions in tuning HIN is strongly correlated with the ion-specific effect on structural transformation from liquid-like to ice-like water (Figure 2A).[2] The structure of interfacial water is determined by the type and amount of counterions distributed at the solid/water interface.[19] The ice nucleation efficiency increases with the fraction of ice-like water molecules. Therefore, the HIN temperature (T_H) is higher on the surface with counterions having greater capability of inducing ice-like water.[2] The T_H on the anti-icing hydrogel surface is the temperature when the ice nucleus appears. The value of T_H is very close to that of freezing temperature of the whole water droplet if the cooling rate is not so fast (for details see Experimental Procedures). We propose that the T_H on these anti-icing hydrogels can be regulated over a large window by using different counterions in the gel network. As shown in Figures 2B and S6, the T_H on the PG1-I hydrogel surface is −17.7°C, whereas it is −29.9°C on the same surface when the counterion is perfluorooctanoate (PFO). The ice nucleation preferentially occurs on the PG1-I hydrogel surface because the counterions of iodine can promote the formation of ice-like water molecules at the hydrogel/water interface, thus enhancing the efficiency of ice nucleation.[19] Although the order of counterions in determining ice nucleation is independent of the film thickness, the difference in T_H is significantly amplified as the thickness increases (Figure 2C). The ion-specific effect in tuning T_H decreases gradually along with the incorporation of long-chain PDMS macromonomers (Figure 2D). The ion specificity completely disappears on PG3 hydrogel surface. The complete series of counterions in tuning T_H was verified on PG1 hydrogel surface, showing a broad tunable T_H window of 12°C (Figure 2E). The inhibition of ice nucleation efficiency of PG1-PFO surfaces is comparable with that of the AFPs (Figure S7). The HIN delay time (t_D) on the PG1 hydrogel surface further consolidates the efficiency of different counterions in tuning T_H (Figure 2F). The t_D of most anti-icing surfaces was measured in the freezing temperature range of −10°C to −20°C.[1,39–41] We studied the freezing delays of PG1-PFO hydrogel surface at ultralow temperatures and found that the PG1-PFO hydrogel surface remained unfrozen for more than 4,800 s even at −28°C, exhibiting high performance of inhibiting ice nucleation.

In real-world environments, sometimes the undesired HIN is inevitable due to the contaminants, dusts, surface edges, and defects, giving rise to ice propagation across the entire surface.[42,43] In addition to ice nucleation, the subsequent ice propagation also plays an important role in ice formation on foreign surfaces. The ice propagation rate, which is the change of ice cover area per unit time during the ice propagation process, was used to quantify the ice propagation inhibition

Please cite this article in press as: He et al., Bioinspired Multifunctional Anti-icing Hydrogel, Matter (2019), https://doi.org/10.1016/j.matt.2019.12.017

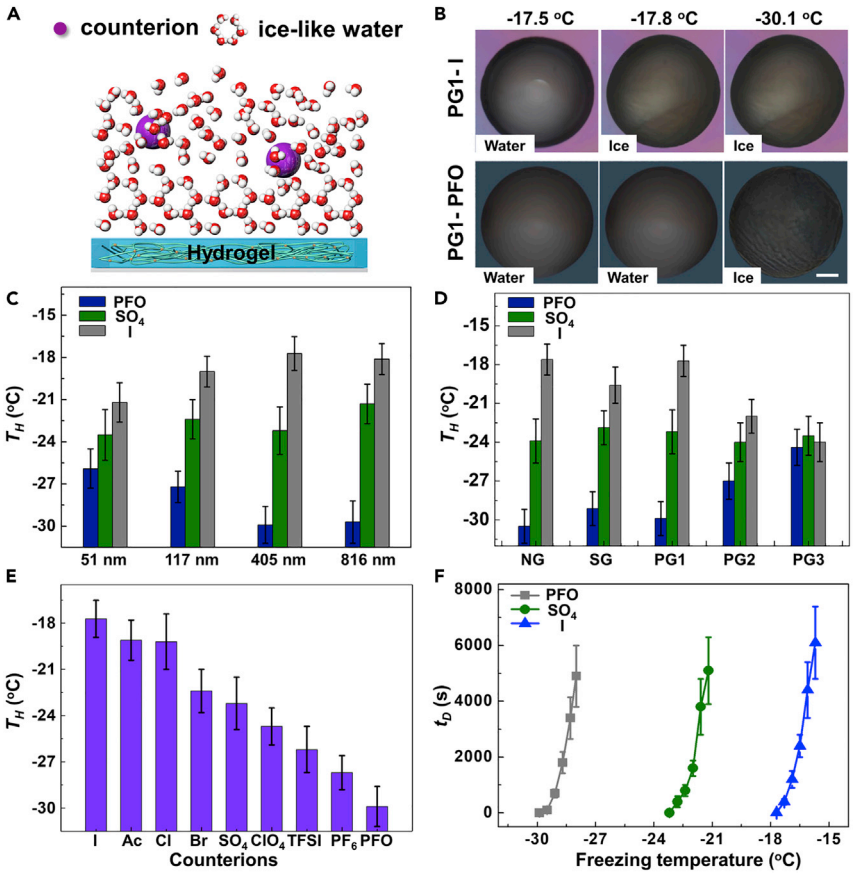

Figure 2. Inhibition of Heterogeneous Ice Nucleation

(A) Ice-like interfacial water on the anti-icing hydrogel with different counterions.

(B) Polarized optical microscopic images of water droplet freezing at different temperatures on PG1 surfaces with counterion of iodide (I^-) and perfluorooctanoate (PFO^-). Scale bar, 200 μm.

(C) Influence of film thickness on the T_H of PG1-I, PG1-SO_4, and PG1-PFO surfaces. Data are presented as mean ± SEM.

(D) T_H on various anti-icing hydrogels with counterions of I^-, SO_4^{2-}, and PFO^-. Data are presented as mean ± SEM.

(E) T_H on PG1 hydrogel with different counterions. Data are presented as mean ± SEM.

(F) Freezing delay time (t_D) on PG1 hydrogel with counterions of I^-, SO_4^{2-}, and PFO^-. Data are presented as mean ± SEM.

efficiency of various coatings. We discovered that ice propagation on a hydrated surface is strongly determined by the amount of interfacial water, that is, more interfacial water results in a higher ice propagation rate (Figure 3A).[19,42] Essentially, the amount of interfacial water can be controlled by tuning the hydrophobicity (via tuning PDMS chain length) to balance the counterions. Since there is also an ion-specific effect on tuning interfacial water amount, i.e., the counterion-driven "hydrophobic collapse," we have investigated the ice propagation rates on various hydrogel surfaces with different counterions. When the PG1 hydrogel undergoes a transition from hydrophilic to hydrophobic state by exchanging I^- with PFO^-, the propagation time (the area is 3.3×10^5 μm^2) increases from 30 to 1,680 ms (Figures 3B and 3C). The ice propagation time (the area is 3.3×10^5 μm^2) on PG1 surface can be tuned by up to two orders of magnitude by changing different counterions (Figure 3D). To exclude the influence of different T_H of various hydrogel surfaces, we performed all ice propagation measurements at −15.0°C. Note that when the PDMS chains

Please cite this article in press as: He et al., Bioinspired Multifunctional Anti-icing Hydrogel, Matter (2019), https://doi.org/10.1016/j.matt.2019.12.017

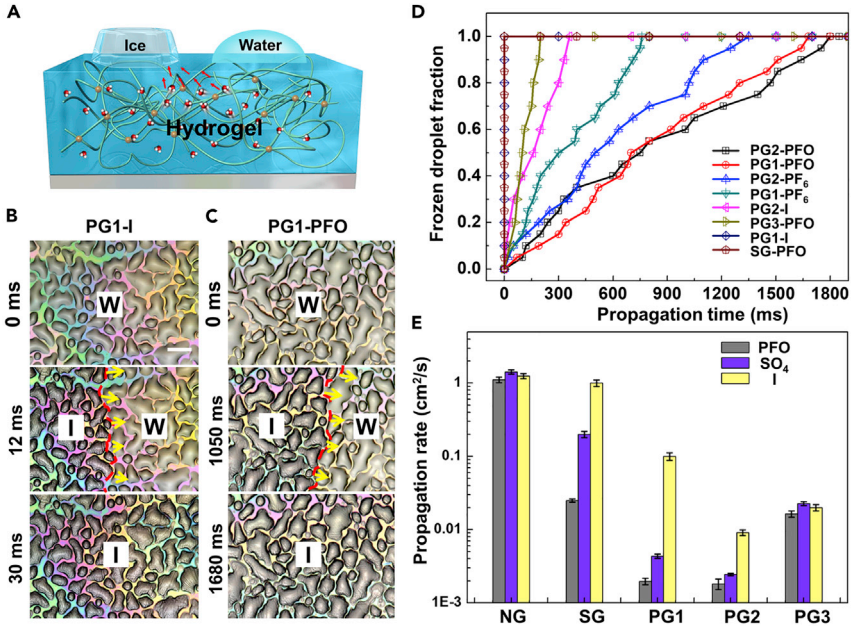

Figure 3. Prevention of Ice Propagation

(A–C) Illustration of ice propagation on the anti-icing hydrogel surface (A). Time-resolved optical microscopic images of ice propagation on the (B) PG1-I and (C) PG1-PFO hydrogel surfaces. I, ice; W, water. Scale bar, 100 μm.

(D) Change of fraction of frozen droplets on various anti-icing hydrogel surfaces with different counterions versus ice propagation time.

(E) Ice propagation rate on various anti-icing hydrogels with counterions of I^-, SO_4^{2-}, and PFO^-. Data are presented as mean ± SEM.

are too long (PG3), the water molecules cannot penetrate into the hydrogel, which will not be tuned by ions; the surfaces can no longer inhibit the ice propagation effectively, similar to the conventional pure PDMS surfaces (Figure 3E). In contrast to the PGs with longer-chain PDMS (PG1 and PG2), the amounts of interfacial water in NG and SG are overly high, even with the presence of the highly hydrophobic counterion of PFO^-. This indicates that the hydrophobicity, which can be tuned by PDMS chain lengths, plays a crucial role in modulating the amounts of interfacial water. As a result, the ultrahigh ice propagation rate caused by an excess amount of interfacial water keeps the NG and SG hydrogels from becoming multifunctional anti-icing materials. This experiment proves that only synergetic cooperation of hydrophobicity and ion specificity can lead to effective control of ice propagation.

If ice forms inevitably in extremely low-temperature environments, reducing ice adhesion will be considered as the last resort. Inspired by ice skating, the interfacial water can serve as an aqueous lubricating layer to reduce the ice adhesion strength (Figure 4A).[2,21] For unmodified hydrogel, the frozen water molecules make ice form through the inside and outside of hydrogel, leading to high ice adhesion strength (the value of ice adhesion strength, τ_{ice}, is higher than 200 kPa). The introduction of grafted PDMS chains helps retain the unfrozen interfacial water as a lubricating layer.[41,44] In comparison with NG, the ice adhesion strengths of PG1–PG3 hydrogels are lower by more than one order of magnitude (Figure 4B). We studied the ice adhesion behavior of the PG1-PFO surface and found that the ice adhesion strength decreases as hydrogel film thickness increases, due to the increased thickness of the viscous lubricating layer (Figure 4C). The unmodified hydrogel of NG is prone to

Please cite this article in press as: He et al., Bioinspired Multifunctional Anti-icing Hydrogel, Matter (2019), https://doi.org/10.1016/j.matt.2019.12.017

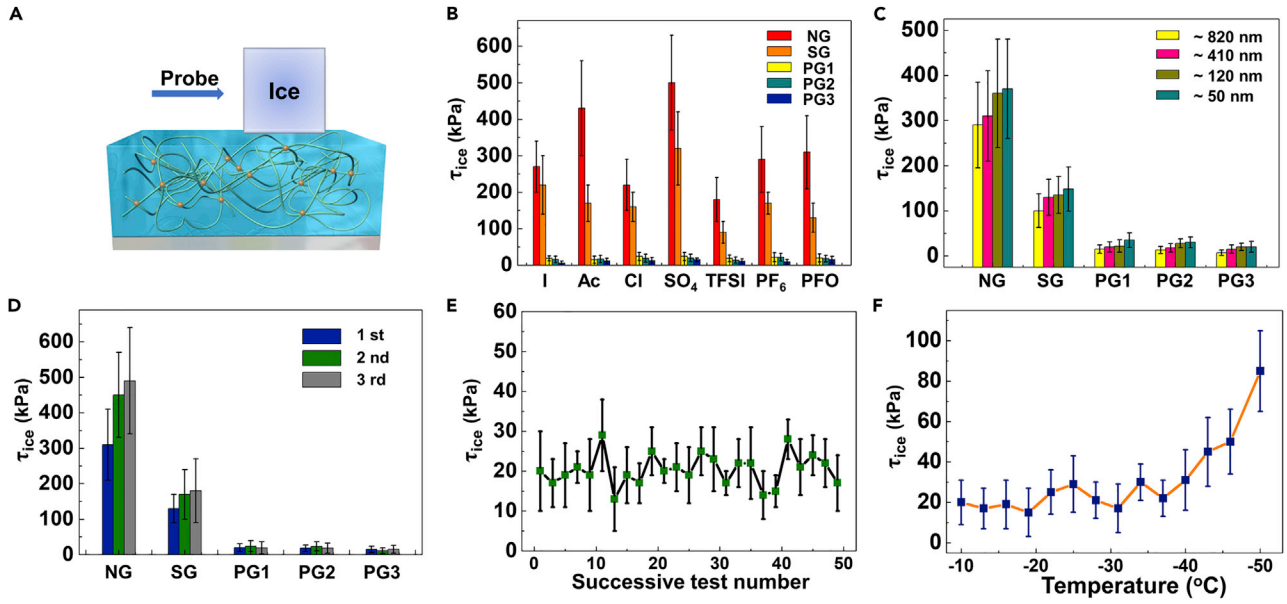

Figure 4. Reduction of Ice Adhesion

(A) Illustration of detecting ice adhesion strength (τ_{ice}).

(B) τ_{ice} on various anti-icing hydrogels with different counterions. Data are presented as mean ± SD.

(C) τ_{ice} on various anti-icing hydrogels (the counterion is PFO^-) with different thicknesses. Data are presented as mean ± SD.

(D) τ_{ice} for various surfaces in three repeated icing/de-icing tests. Data are presented as mean ± SD.

(E) τ_{ice} on PG1-PFO surface after 50 icing/de-icing cycles. Data are presented as mean ± SD.

(F) τ_{ice} on PG1-PFO surface at different temperatures. Data are presented as mean ± SD.

damage when subjected to a de-icing test, and the ice adhesion strength increases significantly in three repeated icing/de-icing tests (Figures 4D and S8). By strong contrast, these PDMS-modified hydrogels including PG1-PFO, PG2-PFO, and PG3-PFO coatings exhibit much higher mechanical robustness and long-term durability. Figure 4E shows that the ice adhesion strength on PG1-PFO hydrogel maintains a low value even after 50 icing/de-icing cycles. However, this PDMS-modified hydrogel of PG1-PFO is still soft matter, and the surface scratches can still be observed through rigorous mechanical abrasion tests as shown in Figure S9. As the temperature is lower than −40°C, the gradual freezing of the lubricating water layer at the PG1-PFO hydrogel interface causes the increase in ice adhesion strength (Figure 4F).

Owing to the excellent properties of inhibiting ice formation and reducing ice adhesion, the PG1-PFO hydrogel stands out to serve as an ideal choice for broad applicability of anti-icing. To meet the various anti-icing/frosting application needs, it is also critical to coat and test PG1-PFO on different substrates. High scalability of the hydrogel fabrication process allows PG1-PFO to be coated on a wide range of devices (Figures S10 and S11). The ice formation and ice adhesion behaviors on different substrates are further demonstrated, showing a promising method to integrate comprehensive icephobic functions into existing surfaces. Figure 5A compares the ice formation times on various coated and uncoated surfaces including metals, ceramic, glass, and polymers. The ice formation time on PG1-PFO hydrogel includes both ice nucleation and propagation time (Figures S12 and S13). All the uncoated surfaces form ice immediately at −25°C, while the PG1-PFO coated surfaces remain unfrozen for more than 3,000 s under the same conditions. Moreover, the ice adhesion strength deceases dramatically when PG1-PFO is coated on various substrates

Please cite this article in press as: He et al., Bioinspired Multifunctional Anti-icing Hydrogel, Matter (2019), https://doi.org/10.1016/j.matt.2019.12.017

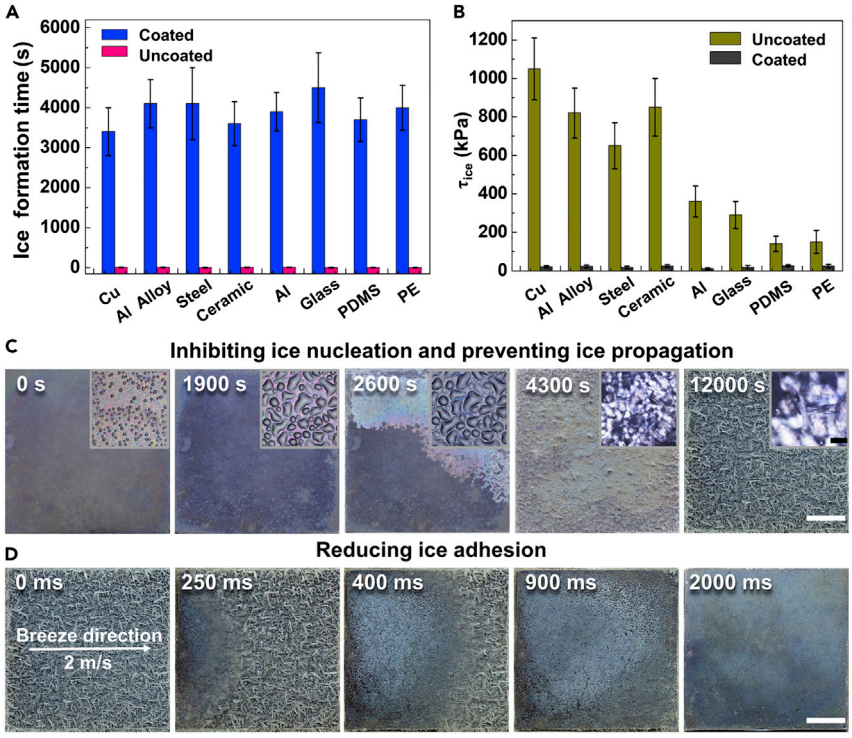

Figure 5. Anti-icing Applications

(A) Ice formation time on various substrates at −25°C before and after coating with PG1-PFO hydrogel. Data are presented as mean ± SD.

(B) τ_{ice} on various substrates before and after coating with PG1-PFO hydrogel. Data are presented as mean ± SD.

(C) Ice formation on the PG1-PFO surface for different times at −25°C when the supersaturation is 106%. Scale bar, 1 cm. Inset scale bar, 200 μm.

(D) The ice formed at −25°C on the PG1-PFO surface is blown off by a breeze. Scale bar, 1 cm.

(Figure 5B). The workability of PG1-PFO coating for de-icing was tested in real environments at −25°C (Figures 5C and 5D). Due to the ice nucleation inhibition on the PG1-PFO surface, water condenses and coarsens for more than 1,900 s. After ice nucleation, the ice propagates slowly via ice bridging. The whole surface is covered with ice in about 4,000s, after which the ice layer thickens with time. For most icephobic surfaces with ultralow ice adhesion strength, air flow is always a feasible measure to remove ice.[42,45] Owing to the low ice adhesion on the PG1-PFO surface, the ice can be blown off easily by a breeze (2 m/s wind speed) within 2 s.

Conclusion

Developing an effective icephobic surface with multiple anti-icing functions through simple design and large-scale production is highly desirable. Inspired by biological AFPs, interfacial water provides us a promising route to integrate advantages of various icephobic materials into PDMS-grafted polyelectrolyte hydrogels. All the effective anti-icing performances are achieved by tuning the properties of interfacial water. We develop a straightforward but effective method to introduce hydrophilic electrolyte and hydrophobic PDMS macromonomers into PG hydrogel coating. It is found that the tunable synergy of hydrophobicity and ion specificity enables a PG1-PFO hydrogel composite surface with high capabilities of tuning ice nucleation, propagation, and adhesion. The subsequent application tests show that these

Please cite this article in press as: He et al., Bioinspired Multifunctional Anti-icing Hydrogel, Matter (2019), https://doi.org/10.1016/j.matt.2019.12.017

multifunctional anti-icing surfaces can delay ice formation remarkably without altering its original ultralow ice adhesion. The broad applicability on a wide range of substrates will open up more opportunities and possibilities for multifunctional anti-icing hydrogels to become promising coatings for icephobicity. Compared with the multifunctional anti-icing properties, the mechanical robustness of this hydrogel coating is less prominent, which may limit its widespread application in real-life conditions. The development of an anti-icing hydrogel that has extraordinary mechanical properties such as double-network hydrogels, inorganic/hydrogel hybrids, and hydrogel fibers is still urgently needed,.

EXPERIMENTAL PROCEDURES

Materials

[2-(Methacryloyloxy)ethyl]trimethylammonium chloride (PMETAC), sodium hexafluorophosphate, sodium perchlorate, sodium perfluorooctanoate, bis(trifluoromethane) sulfonamide lithium, sodium iodide, sodium sulfate, sodium bromide, sodium acetate, 2-hydroxy-4′-(2-hydroxyethoxy)-2-methylpropiophenone (Irgacure 2959) and 3-(trimethoxysilyl)propyl methacrylate (TMSPMA) were all purchased from Sigma-Aldrich. Mono-methacryloxypropyl terminated polydimethylsiloxane (PDMS) of various molecular weights was purchased from Gelest. Silicon wafers were purchased from Waferpro. The polymer of poly(AAm-co-AAc-co-AAene) were synthesized using same procedure as described previously.[32]

Fabrication of Polydimethylsiloxane-Grafted Polyelectrolyte Hydrogel

The precursor solution contained 2 wt % poly(AAm-co-AAc-co-AAene), 0.5 wt % PMETAC, 0.5 wt % mono-methacryloxypropyl terminated PDMS with various molecular weights, and 0.3% initiator of Irgacure 2959 in 50% acetic acid/water solution. The prepared precursor solution of hydrogel was spin-coated onto silicon substrate with UV exposure. The vinyl-functioned silicon substrates were modified with TMSPMA. The PDMS-grafted polyelectrolyte hydrogels were fabricated via *in situ* polymerization. The samples were washed with Milli-Q water and alcohol to remove the unreacted precursor.

Counterion Exchange

The Cl^- in PMETAC monomer was exchanged by immersing the hydrogel samples into 0.5-M salt solutions of target counteranions for 30 min. The films were then washed with Milli-Q water to remove excess free salts on the surface. The success of counterion exchange was confirmed by measurements of XPS.

Surface Characterization

The hydrogel film thicknesses were calculated from the UV-visible reflective spectrum by using the same methods as the previous works. The static contact angles were measured by a drop size analyzer (DSA-100; Krüss, Germany). The structures of various PDMS-grafted polyelectrolyte hydrogels were detected by Fourier transform infrared spectroscopy. The copolymerization and ion exchange were detected by XPS measurements. The morphologies of different PDMS-grafted polyelectrolyte hydrogel surfaces before and after ice adhesion tests were detected by an atomic force microscope (Bruker Multimode 8).

Ice Nucleation Measurement

The HIN temperature (T_H) and ice nucleation delay time (t_D) on various PDMS-grafted polyelectrolyte hydrogel surfaces were measured by an optical microscope coupled with a high-speed camera (Phantom v7.3). The resolution of the high-speed camera is 0.1 ms (10^4 frames/s). The cooling processes were regulated by a cryostage (Linkam

THMS 600). The temperature resolution of T_H was less than 0.1°C. The T_H on anti-icing hydrogel surface is the temperature when the ice nucleus appears. The ice nucleus on nanoscale cannot be observed by the optical microscope. However, the freezing of the whole water droplet can be observed by detecting the change of opacity before and after droplet freezing. The freezing time for a whole water droplet is shorter than 1 s. When the cooling rate is 5°C/min, the temperature error between freezing temperature of whole droplet and T_H is lower than 0.1°C. Therefore, the value of T_H is almost the same as that of freezing temperature of the whole water droplet if the cooling rate is not so fast (the cooling rate is 2°C/min in this work). The t_D was the delay time when these multifunctional anti-icing hydrogel surfaces reached objective temperatures before freezing. The data of the T_H and t_D represented the statistical average of more than 200 freezing events for each hydrogel sample. The error bar was determined by the standard error of the mean (SEM).

Ice Propagation Measurement

The ice propagation rate (time) of condensed water on various PDMS-grafted polyelectrolyte hydrogels were measured by an optical microscope coupled with a high-speed camera. The condensed water droplets formed on the hydrogel surface via "evaporation and condensation processes" in a closed cell. The relative humidity in the sample cell was controlled at 100%. To exclude the influence of different T_H of various hydrogel surfaces with different counterions, we performed all of the ice propagation measurements at −15.0°C, and the initial ice propagations were triggered by a frozen AgI droplet.[42] The fractions of frozen water droplets were analyzed by ImageJ software.

Ice Adhesion Measurement

The ice adhesion strength was measured on a cooling stage coupled with an XY motion stage and a force transducer. Each datum of ice adhesion strength on various PDMS-grafted polyelectrolyte hydrogels was averaged over ten individual measurements. The nitrogen gas was purged into the closed sample cell to minimize the effect of frost formation. The tests were performed at various temperatures when the water froze completely. A cylindrical water container was used to minimize the effect of stress concentration.

Ice Formation Time Measurement

The ice formation time on PDMS-grafted polyelectrolyte hydrogel surface includes both ice nucleation and ice propagation time. The ice formation time was measured via an optical microscope coupled with a high-speed camera. The ice formation time on various substrates coated with PDMS-grafted polyelectrolyte hydrogel was measured at −25°C.

Multifunctional Anti-icing Hydrogel Coated on Various Surfaces

Various surfaces including metals, ceramics, glass, and polymers were vinyl-functioned by dopamine methacrylamide (DMA). All of the different substrates were washed by isopropanol and deionized water and then treated with oxygen plasma. The prepared substrates were dip-coated into an aqueous solution of DMA (2 mg/mL) for 12 h. Thereafter the substrates were washed with Milli-Q water and completely dried.

DATA AND CODE AVAILABILITY

All data needed to evaluate the conclusions in the paper are present in the paper and/or the Supplemental Information. Additional data related to this paper may be requested from the authors.

SUPPLEMENTAL INFORMATION

Supplemental Information can be found online at https://doi.org/10.1016/j.matt.2019.12.017.

ACKNOWLEDGMENTS

The authors are grateful for the financial support from the Youth Innovation Promotion Association of the Chinese Academy of Sciences, China (2018044), AFOSR grant, United States (FA9550-17-1-0311), the NSF CAREER award, United States (1724526), the Hellman Fellows Funds, United States, and the Chinese National Natural Science Foundation of China, China (21875261 and 21733010).

AUTHOR CONTRIBUTIONS

Z.H., X.Z., J.W., and X.H. initiated the idea of multifunctional anti-icing materials and supervised the experiments. Z.H. and C.W. designed and carried out the experiments. S.W., M.H., and D.W. measured the ice nucleation efficiency. Z.H., X.Z., J.W., and X.H. wrote the initial draft of the manuscript. All of the authors contributed to the analysis of the data and modification of the manuscript.

DECLARATION OF INTERESTS

The authors declare that they have no competing interests.

Received: September 20, 2019
Revised: October 29, 2019
Accepted: December 12, 2019
Published: January 29, 2020

REFERENCES

1. Kreder, M.J., Alvarenga, J., Kim, P., and Aizenberg, J. (2016). Design of anti-icing surfaces: smooth, textured or slippery? Nat. Rev. Mater. *1*, 15003.
2. He, Z., Liu, K., and Wang, J. (2018). Bioinspired materials for controlling ice nucleation, growth, and recrystallization. Acc. Chem. Res. *51*, 1082–1091.
3. Chatterjee, R., Beysens, D., and Anand, S. (2019). Delaying ice and frost formation using phase-switching liquids. Adv. Mater. *31*, e1807812.
4. Walker, C., Lerch, S., Reininger, M., Eghlidi, H., Milionis, A., Schutzius, T.M., and Poulikakos, D. (2018). Desublimation frosting on nanoengineered surfaces. ACS Nano *12*, 8288–8296.
5. Boreyko, J.B., and Collier, C.P. (2013). Delayed frost growth on jumping-drop superhydrophobic surfaces. ACS Nano *7*, 1618–1627.
6. Laforte, J.L., Allaire, M.A., and Laflamme, J. (1998). State-of-the-art on power line de-icing. Atmos. Res. *46*, 143–158.
7. Bartels-Rausch, T. (2013). Chemistry: ten things we need to know about ice and snow. Nature *494*, 27–29.
8. Boinovich, L.B., Emelyanenko, A.M., Emelyanenko, K.A., and Modin, E.B. (2019). Modus operandi of protective and anti-icing mechanisms underlying the design of longstanding outdoor icephobic coatings. ACS Nano *13*, 4335–4346.
9. Ahmadi, S.F., Nath, S., Iliff, G.J., Srijanto, B.R., Collier, C.P., Yue, P., and Boreyko, J.B. (2018). Passive antifrosting surfaces using microscopic ice patterns. ACS Appl. Mater. Interfaces *10*, 32874–32884.
10. Lv, J., Song, Y., Jiang, L., and Wang, J. (2014). Bio-inspired strategies for anti-icing. ACS Nano *8*, 3152–3169.
11. Kim, P., Wong, T., Alvarenga, J., Kreder, M.J., Adorno-Martinez, W.E., and Aizenberg, J. (2012). Liquid-infused nanostructured surfaces with extreme anti-ice and anti-frost performance. ACS Nano *6*, 6569–6577.
12. Anand, S., Paxson, A.T., Dhiman, R., Smith, J.D., and Varanasi, K.K. (2012). Enhanced condensation on lubricant-impregnated nanotextured surfaces. ACS Nano *6*, 10122–10129.
13. Guo, Q., He, Z., Jin, Y., Zhang, S., Wu, S., Bai, G., Xue, H., Liu, Z., Jin, S., and Zhao, L. (2018). Tuning ice nucleation and propagation with counterions on multilayer hydrogels. Langmuir *34*, 11986–11991.
14. Golovin, K., and Tuteja, A. (2017). A predictive framework for the design and fabrication of icephobic polymers. Sci. Adv. *3*, e1701617.
15. Golovin, K., Kobaku, S.P., Lee, D.H., DiLoreto, E.T., Mabry, J.M., and Tuteja, A. (2016). Designing durable icephobic surfaces. Sci. Adv. *2*, e1501496.
16. Wong, T.S., Kang, S.H., Tang, S.K.Y., Smythe, E.J., Hatton, B.D., Grinthal, A., and Aizenberg, J. (2011). Bioinspired self-repairing slippery surfaces with pressure-stable omniphobicity. Nature *477*, 443–447.
17. Farhadi, S., Farzaneh, M., and Kulinich, S.A. (2011). Anti-icing performance of superhydrophobic surfaces. Appl. Surf. Sci. *257*, 6264–6269.
18. Kulinich, S.A., and Farzaneh, M. (2009). How wetting hysteresis influences ice adhesion strength on superhydrophobic surfaces. Langmuir *25*, 8854–8856.
19. He, Z., Xie, W.J., Liu, Z., Liu, G., Wang, Z., Gao, Y.Q., and Wang, J. (2016). Tuning ice nucleation with counterions on polyelectrolyte brush surfaces. Sci. Adv. *2*, e1600345.
20. Liu, Z., He, Z., Lv, J., Jin, Y., Wu, S., Liu, G., Zhou, F., and Wang, J. (2017). Ion-specific ice propagation behavior on polyelectrolyte brush surfaces. RSC Adv. *7*, 840–844.
21. Chen, J., Luo, Z., Fan, Q., Lv, J., and Wang, J. (2014). Anti-ice coating inspired by ice skating. Small *10*, 4693–4699.
22. Dou, R., Chen, J., Zhang, Y., Wang, X., Cui, D., Song, Y., Jiang, L., and Wang, J. (2014). Anti-icing coating with an aqueous lubricating layer. ACS Appl. Mater. Interfaces *6*, 6998–7003.

23. Golovin, K., Dhyani, A., Thouless, M.D., and Tuteja, A. (2019). Low-interfacial toughness materials for effective large-scale deicing. Science *364*, 371–375.

24. Wu, S., He, Z., Zang, J., Jin, S., Wang, Z., Wang, J., Yao, Y., and Wang, J. (2019). Heterogeneous ice nucleation correlates with bulk-like interfacial water. Sci. Adv. *5*, eaat9825.

25. Shen, Y., Wu, Y., Tao, J., Zhu, C., Chen, H., Wu, Z., and Xie, Y. (2018). Spraying fabrication of durable and transparent coatings for anti-icing application: dynamic water repellency, icing delay, and ice adhesion. ACS Appl. Mater. Interfaces *11*, 3590–3598.

26. DeVries, A.L., and Wohlschlag, D.E. (1969). Freezing resistance in some Antarctic fishes. Science *163*, 1073–1075.

27. Nutt, D.R., and Smith, J.C. (2008). Dual function of the hydration layer around an antifreeze protein revealed by atomistic molecular dynamics simulations. J. Am. Chem. Soc. *130*, 13066–13073.

28. Liou, Y.C., Tocilj, A., Davies, P.L., and Jia, Z. (2000). Mimicry of ice structure by surface hydroxyls and water of a beta-helix antifreeze protein. Nature *406*, 322–324.

29. Liu, K., Wang, C., Ma, J., Shi, G., Yao, X., Fang, H., Song, Y., and Wang, J. (2016). Janus effect of antifreeze proteins on ice nucleation. Proc. Natl. Acad. Sci. U S A *113*, 14739–14744.

30. Hudait, A., Qiu, Y., Odendahl, N., and Molinero, V. (2019). Hydrogen-bonding and hydrophobic groups contribute equally to the binding of hyperactive antifreeze and ice-nucleating proteins to ice. J. Am. Chem. Soc. *141*, 7887–7898.

31. Chen, J., Dou, R., Cui, D., Zhang, Q., Zhang, Y., Xu, F., Zhou, X., Wang, J., Song, Y., and Jiang, L. (2013). Robust prototypical anti-icing coatings with a self-lubricating liquid water layer between ice and substrate. ACS Appl. Mater. Interfaces *5*, 4026–4030.

32. Qin, M., Sun, M., Bai, R., Mao, Y., Qian, X., Sikka, D., Zhao, Y., Qi, H.J., Suo, Z., and He, X. (2018). Bioinspired hydrogel interferometer for adaptive coloration and chemical sensing. Adv. Mater. *30*, e1800468.

33. Sun, M., Bai, R., Yang, X., Song, J., Qin, M., Suo, Z., and He, X. (2018). Hydrogel interferometry for ultrasensitive and highly selective chemical detection. Adv. Mater. *30*, e1804916.

34. Huber, R.O., Beebe, J.M., Smith, P.B., Howell, B.A., and Ahn, D. (2018). Facile synthesis of thermoresponsive poly(NIPAAm-g-PDMS) copolymers using room temperature alkylborane chemistry. Macromolecules *51*, 4259–4268.

35. He, Z., Zheng, L., Liu, Z., Jin, S., Li, C., and Wang, J. (2017). Inhibition of heterogeneous ice nucleation by bioinspired coatings of polyampholytes. ACS Appl. Mater. Interfaces *9*, 30092–30099.

36. Fitzner, M., Sosso, G.C., Cox, S.J., and Michaelides, A. (2015). The many faces of heterogeneous ice nucleation: interplay between surface morphology and hydrophobicity. J. Am. Chem. Soc. *137*, 13658–13669.

37. Mishchenko, L., Hatton, B., Bahadur, V., Taylor, J.A., Krupenkin, T., and Aizenberg, J. (2010). Design of ice-free nanostructured surfaces based on repulsion of impacting water droplets. ACS Nano *4*, 7699–7707.

38. Graeber, G., Schutzius, T.M., Eghlidi, H., and Poulikakos, D. (2017). Spontaneous self-dislodging of freezing water droplets and the role of wettability. Proc. Natl. Acad. Sci. U S A *114*, 11040–11045.

39. Wang, L., Gong, Q., Zhan, S., Jiang, L., and Zheng, Y. (2016). Robust anti-icing performance of a flexible superhydrophobic surface. Adv. Mater. *28*, 7729–7735.

40. Alizadeh, A., Yamada, M., Li, R., Shang, W., Otta, S., Zhong, S., Ge, L., Dhinojwala, A., Conway, K.R., Bahadur, V., et al. (2012). Dynamics of ice nucleation on water repellent surfaces. Langmuir *28*, 3180–3186.

41. Guo, P., Zheng, Y., Wen, M., Song, C., Lin, Y., and Jiang, L. (2012). Icephobic/anti-icing properties of micro/nanostructured surfaces. Adv. Mater. *24*, 2642–2648.

42. Jin, Y., He, Z., Guo, Q., and Wang, J. (2017). Control of ice propagation via polyelectrolyte multilayer coatings. Angew. Chem. Int. Ed. *56*, 11436–11439.

43. Chen, X., Ma, R., Zhou, H., Zhou, X., Che, L., Yao, S., and Wang, Z. (2013). Activating the microscale edge effect in a hierarchical surface for frosting suppression and defrosting promotion. Sci. Rep. *3*, 2515.

44. Chen, D., Gelenter, M.D., Hong, M., Cohen, R.E., and McKinley, G.H. (2017). Icephobic surfaces induced by interfacial nonfrozen water. ACS Appl. Mater. Interfaces *9*, 4202–4214.

45. Liu, J., Zhu, C., Liu, K., Jiang, Y., Song, Y., Francisco, J.S., Zeng, X.C., and Wang, J. (2017). Distinct ice patterns on solid surfaces with various wettabilities. Proc. Natl. Acad. Sci. U S A *114*, 11285–11290.

Matter, Volume *2*

Supplemental Information

Bioinspired Multifunctional Anti-icing Hydrogel

Zhiyuan He, Chenyang Wu, Mutian Hua, Shuwang Wu, Dong Wu, Xinyuan Zhu, Jianjun Wang, and Ximin He

Supplemental Data

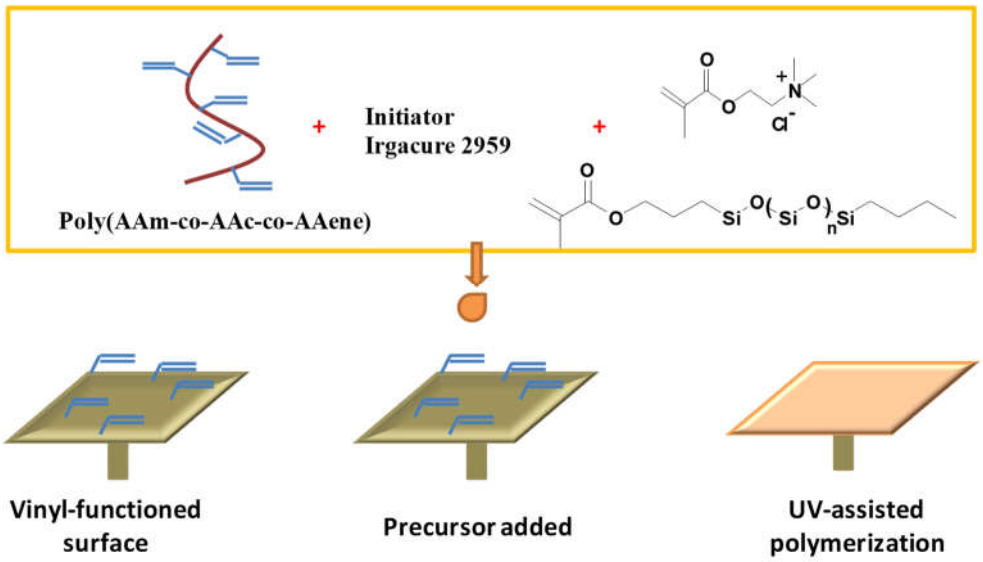

Figure S1. Fabrication of anti-icing PDMS-grafted polyelectrolyte hydrogel surface.

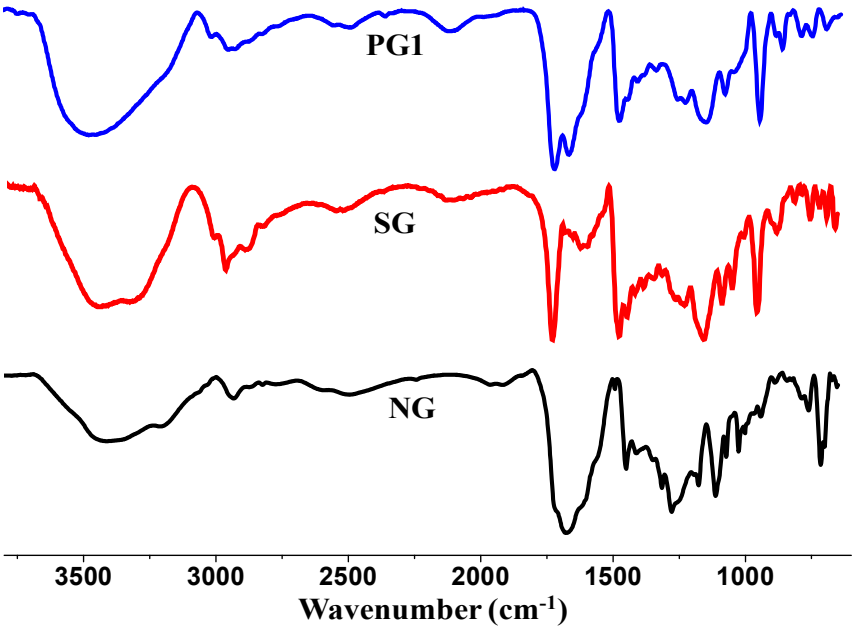

Figure S2. FTIR spectra of various PDMS-grafted polyelectrolyte hydrogel.

Figure S3. Static contact angles of PG1 hydrogel surfaces with different counterions.

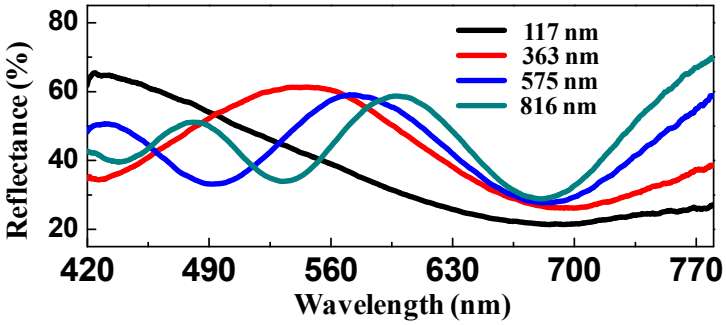

Figure S4. The film thickness of PG1 is detected by reflective spectra.

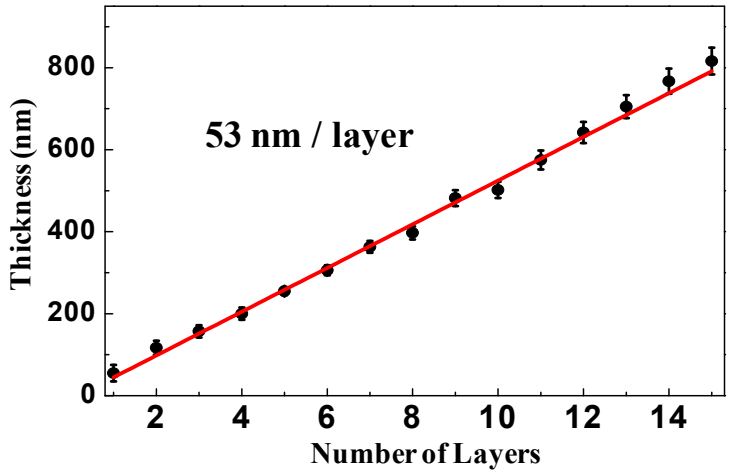

Figure S5. The variation of film thickness vs. the number of spin-coated hydrogel layers.

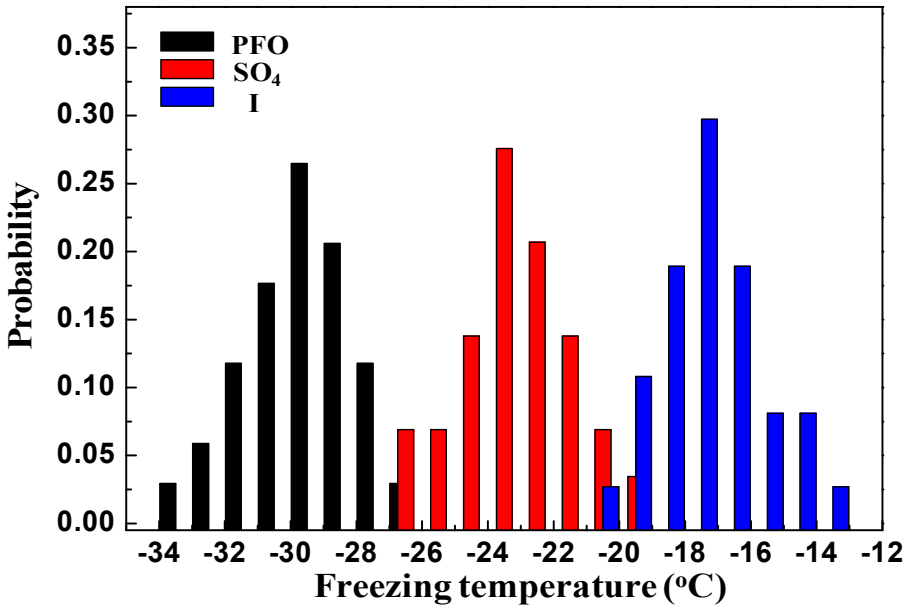

Figure S6. Freezing temperature distribution of PG1 with different counterions.

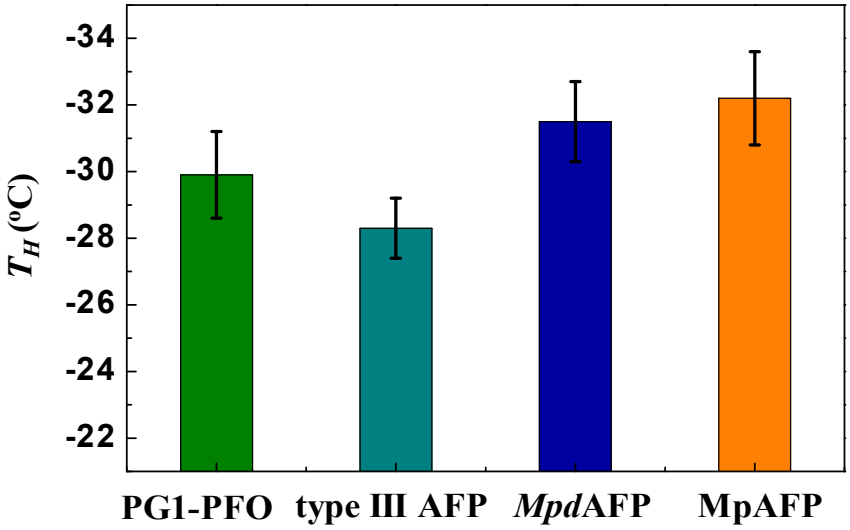

Figure S7. Comparison of T_H of PG1-PFO with different antifreeze proteins (AFPs).

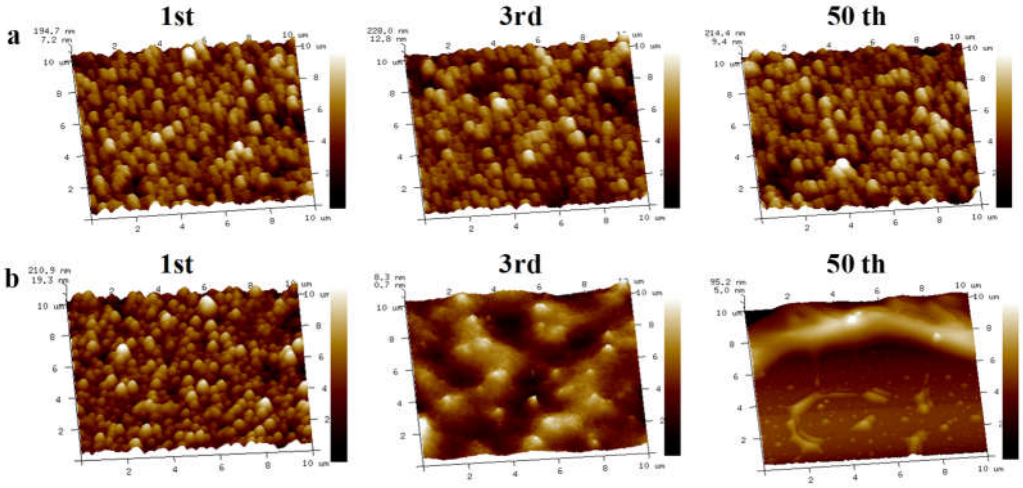

Figure S8. The AFM morphologies of (a) PDMS-modified PG1-PFO hydrogel, and (b) unmodified hydrogel after different repeated icing/deicing tests.

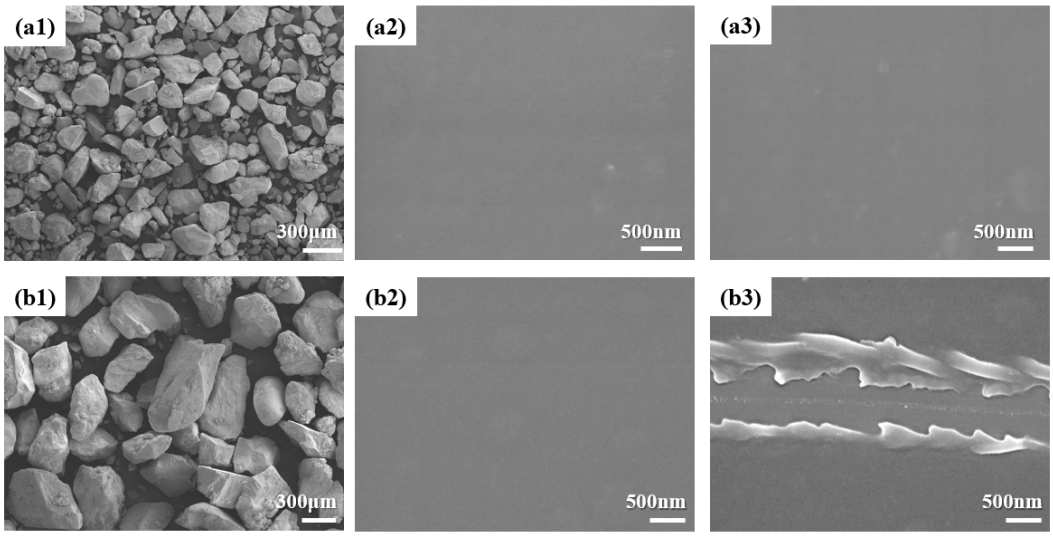

Figure S9. Scanning electron microscopy (SEM) images of PG1-PFO hydrogel surface morphologies after different mechanical abrasion tests with (a) fine sand (particle diameter is smaller than ~300 μm), and (b) coarse sand (particle diameter is about 800-300 μm). The morphologies of (a1) fine sand and (b1) coarse sand. The morphologies of PG1-PFO hydrogel surface (2) before and (3) after mechanical abrasion tests with (a) fine sand and (b) coarse sands. Away from the fall to 0.4 m height, the sand (~10g) fell on the PG1-PFO hydrogel surface, and the impact velocity was about 2.8 m/s. The PG1-PFO hydrogel samples were held at an angle of 45^{o} to the ground. The initial PG1-PFO hydrogel surface is flat and smooth as shown in Fig S9. a2-b2. The fine sand (particle diameter is smaller than ~300 μm) cannot damage the surface, and the morphology of PG1-PFO hydrogel surface is almost the same after mechanical abrasion test (see in Fig S9. a3). However, this PDMS-modified hydrogel of PG1-PFO is still soft matter, and the surface scratches can still be observed through rigorous mechanical abrasion tests as shown in Fig S9. b3.

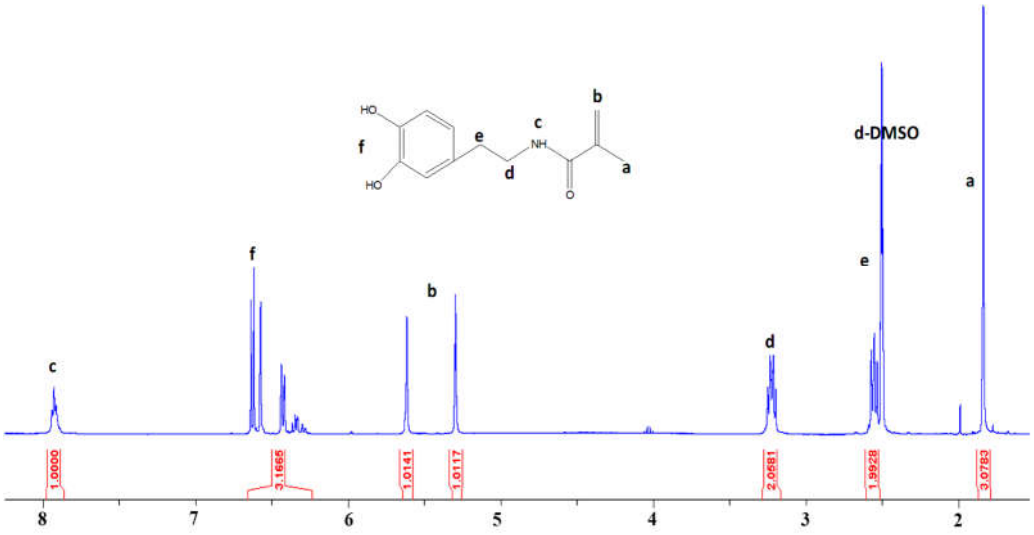

Figure S10. ^{1}H NMR spectrum of dopamine methacrylamide (DMA).

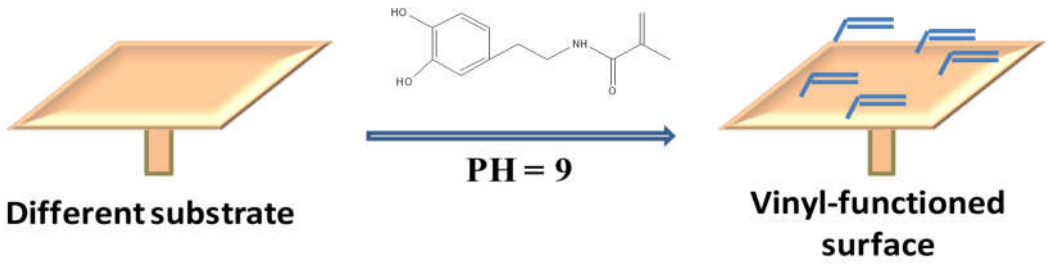

Figure S11. Dopamine methacrylamide (DMA) can be coated onto different inorganic and organic materials, such as metals, plastics, oxides and ceramics.

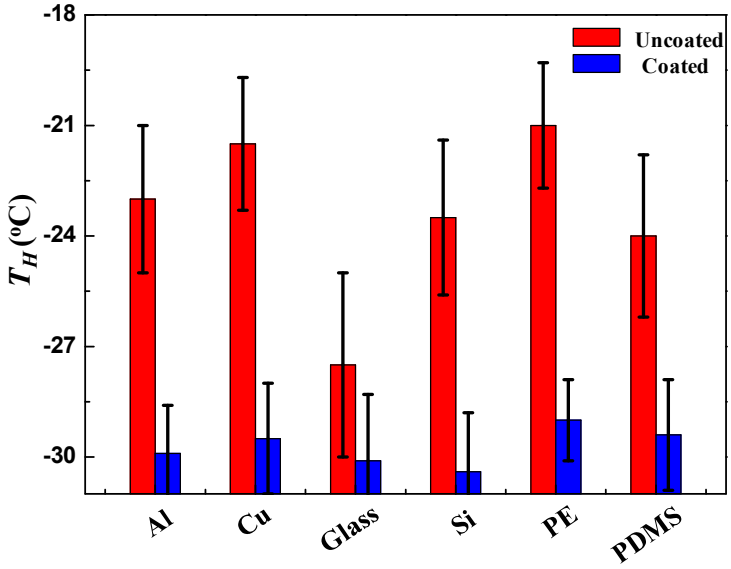

Figure S12. T_H on various PG1-PFO coated and uncoated substrates.

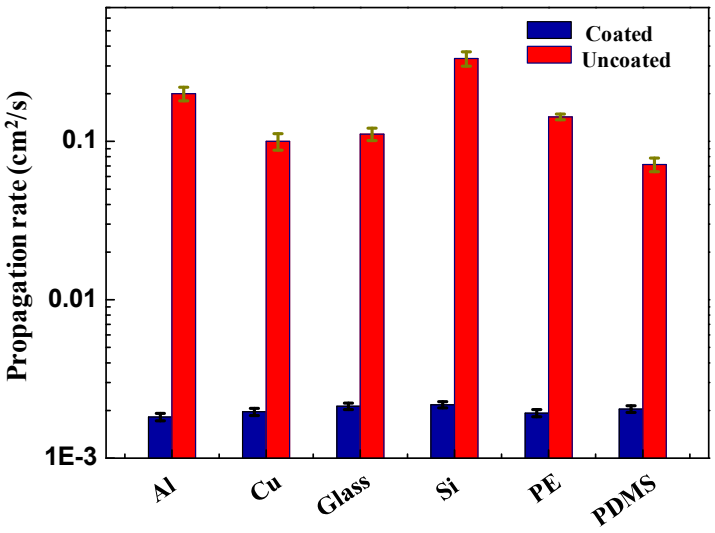

Figure S13. Ice propagation rate on various PG1-PFO coated and uncoated substrates.